

Short Communication

Investigation on the Microstructure and Electrochemical Corrosion Properties of TiB₂ reinforced aluminum matrix composites

Qi-di Wu¹, Xian-ming Meng², Jian-jun Guan¹, Qing Liu^{1,*}, Ping Liang¹, Yinan Wang³

¹ School of Mechanical Engineering, Liaoning Petrochemical University, Fushun 113001, Liaoning, China

² Automotive Engineering Research Institute, China Automotive Technology & Research Center Co. Ltd., Tianjin, 300300, China

³ College of Science, Liaoning Petrochemical University, Fushun 113001, Liaoning, China

*E-mail: 417857491@qq.com

Received: 11 February 2022 / Accepted: 1 April 2022 / Published: 7 May 2022

The TiB₂ particles reinforced AlSi10Mg composites were prepared by selective laser melting (SLM). The effect of TiB₂ particles on the microstructure and electrochemical corrosion properties of the Al-based composites was studied. The phase structure was examined by X-ray diffraction (XRD). The morphology was observed by the metallographic microscope and scanning electron microscope. The corrosion behavior was evaluated by Potentiodynamic polarization and electrochemical impedance spectroscopy. In this experiment, the corrosion resistance of TiB₂ aluminum matrix composites with different contents in 3.5 % NaCl solution at 25 °C (room temperature) was mainly tested. Firstly, the addition of TiB₂ can effectively improve the morphology of the molten pool. Secondly, the addition of TiB₂ will change the corrosion type of Al matrix composites: from uniform / comprehensive corrosion to pitting corrosion, which is easy to occur around TiB₂ particles. Through the experimental data, it was observed that the corrosion potential of the sample was positively shifted by adding TiB₂, and the electrochemical stability was improved. The addition of TiB₂ can effectively reduce the corrosion tendency of the samples. When the content of TiB₂ increases to 5 %, the pitting corrosion occurs seriously, and when TiB₂ is added to 15 %, the corrosion resistance of the samples increases again.

Keywords: SLM, Aluminum matrix composites, TiB₂, Microstructure, Electrochemical corrosion

1. INTRODUCTION

Nowadays, selective laser melting (SLM), a rapid additive manufacturing technology, is widely used to rapidly manufacture lightweight and complex structural parts [1,2]. Selective laser melting (SLM) mainly layers 3D models, then discretizes them, and finally performs layer-by-layer printing to obtain complex structural parts [1,3,4]. So far, many alloys fabricated by selective laser melting (SLM),

such as aluminum alloys and titanium alloys, show good mechanical properties and excellent corrosion resistance compared with alloys fabricated by traditional processes [5-7].

As one of the most widely used aluminum alloys in industry, Al-Si alloy has many advantages such as lightweight, good wear resistance, good thermal expansion coefficient, high specific strength, and good thermal conductivity, so it has been widely used in the automotive and aerospace industries. Application [8]. Rao et al. [9] found that the Si particles combined with tensile properties could be affected by the melt pool and building direction. Mehran Rafieezad et al. [10] studied the application of friction stir machining on the surface of AlSi10Mg alloy prepared by laser-powder-bed fusion to locally modify the alloy structure and enhance the corrosion performance of the alloy. Xinliang Xie et al. successfully fabricated a dense in-situ TiB₂ nanoparticle-enhanced 7075Al composite coating using Cold spray (CS) and evaluated its corrosion resistance using electrochemical methods. At present, few studies have been conducted on the microstructure of Al-based composites with TiB₂ particles added directly by SLM and the effect of TiB₂ particles on the corrosion resistance of the composites [11].

In the work, SLM technology is used to obtain aluminum alloy components with high density and high corrosion resistance by adding different contents of TiB₂ into AlSi10Mg samples. To further improve its comprehensive performance, different contents of TiB₂ were designed for comparison, and the law of the evolution of Al-Si eutectic structure with different contents of TiB₂ was analyzed, and the corrosion properties were discussed to provide a reference for the optimization of the microstructure and corrosion properties of AlSi10Mg samples prepared by SLM.

2. EXPERIMENTAL

2.1 Materials

In the experiment, additively manufactured AlSi10Mg, 5%TiB₂-AlSi10Mg, 15%TiB₂-AlSi10Mg composite materials were used, and AlSi10Mg alloy powder (50 microns in diameter) and TiB₂ (10 microns in diameter) were used. The nominal composition (wt.%) of AlSi10Mg-based alloy is Al-9.5, Si-0.5Mg, and the composites were prepared with 5% volTiB₂ particles and 15% volTiB₂ particles, and then SLM was used to carry a Yb laser on an EOS M280 3D printer, wavelength 1064nm. The samples were obtained under the conditions of a laser scanning speed of 1000 mm/s, an opening distance of 0.13 mm, and a power of 370 W. The chemical composition of AlSi10Mg produced by SLM is listed in Table 1.

Table 1 Compositions of AlSi10Mg (wt.%)

compositions	Si	Mg	Mn	Cu	Fe	Ni	Zn	Sn	Al
content	9.20	0.48	0.21	0.26	0.84	0.17	0.25	0.11	Bal.

2.2 Microstructure characterization

All samples were observed and analyzed using an XJP-6A metallographic microscope. Microscopic characterization of untreated and adding TiB₂ samples were performed using a QUANTA 450 scanning electron microscope (SEM) and energy dispersive spectroscopy (EDS, Oxford instruments). The size, morphology, and distribution of Si particles and TiB₂ particles were analyzed by Image-Pro image analysis software. The phase constituents of all samples were performed by X-ray diffraction (XRD, Bruker D8Advance X-ray diffractometer) with Cu K α radiation (0.15406 nm) at 40 kV and 40 mA. The scanning angle ranged from 20 ° to 100 °, and Jade6.5 software was used for data analysis.

2.3 Electrochemical test process

Electrochemical measurements were performed using an electrochemical workstation (CS350, CorrTest, China). Corrosion of the specimens was tested using a three-electrode system according to ASTM G3-89. Next, write about the electrochemical test piece and size. In the electrochemical test, a platinum electrode was used as the counter electrode (CE), saturated silver/silver chloride (Ag/AgCl) was used as the reference electrode (RE), and the sample (TiB₂-AlSi10Mg Sample with different contents) was used as the working electrode (WE). For each sample, fresh 400 mL of 3.5 wt.% NaCl solution was used while using a water bath to ensure room temperature (25 ± 0.5 °C) during the test.

The open-circuit potential (OCP) was maintained for 1 h for each electrochemical test to ensure that the samples reached a steady state in the test environment. The test parameters for Anodic polarization are a scan rate of 0.125 mV/s and a scan range of -0.02V to 0.3V vs OCP. At least 3 samples were tested to ensure data reproducibility and accuracy. The anodic polarization data were fitted and analyzed using the software CorrTest CS Studio that comes with the electrochemical workstation. The EIS test was also carried out in a 3.5wt.% NaCl solution at room temperature of 25 °C. The EIS test potential was selected as OCP, and the frequency range was 0.01Hz to 100kHz. As with the polarization test, the impedance spectrum was recorded using a sinusoidal potential signal with an amplitude of 10 mV, logarithmically swept every 10 points. Impedance spectra were fitted with ZSimpWin data fitting software.

3. RESULTS AND DISCUSSION

3.1 Phase structure of the TiB₂-AlSi10Mg composites

Figure 1 shows the XRD patterns of SLM forming of TiB₂/AlSi10Mg composites with different contents. The Al phase, Al-Si eutectic phase, and TiB₂ phase were detected in all three samples. Within the detection range of XRD, there are obvious differences in the XRD patterns of the three contents. Among them, the diffraction peaks of the Si phase are weaker, indicating that a large part of the aluminum matrix composites formed by SLM exists in the Al matrix. During the whole SLM process, TiB₂ will affect the Al-Si eutectic phase, and the content of the Al-Si eutectic phase decreases with the increase of TiB₂. This may be because the temperature rises during SLM, and the excessively high

temperature melts the Al matrix, resulting in the existence of TiB_2 instead of part of the Al and Al-Si eutectic phases. It is consistent with the previously reported results of Al-12Si, AlSi10Mg, and their composites prepared by SLM.

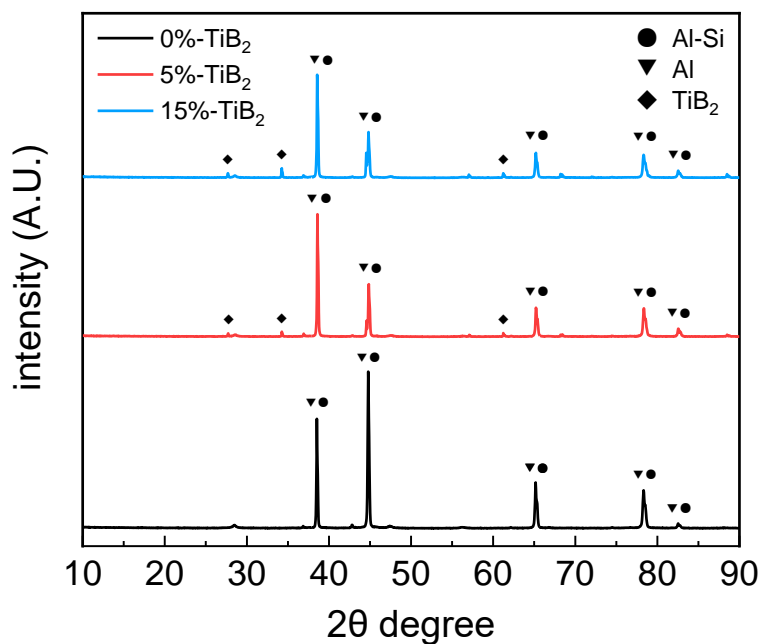


Figure 1. XRD patterns of AlSi10Mg alloys with different TiB_2 contents

3.2 Microstructure of the TiB_2 -AlSi10Mg composites

After the 0%- TiB_2 /AlSi10Mg, 5%- TiB_2 /AlSi10Mg and 15%- TiB_2 /AlSi10Mg samples were corroded, the surfaces of the samples were observed with a metallographic microscope. The schematic diagram of its microstructure is shown in Figure 2.

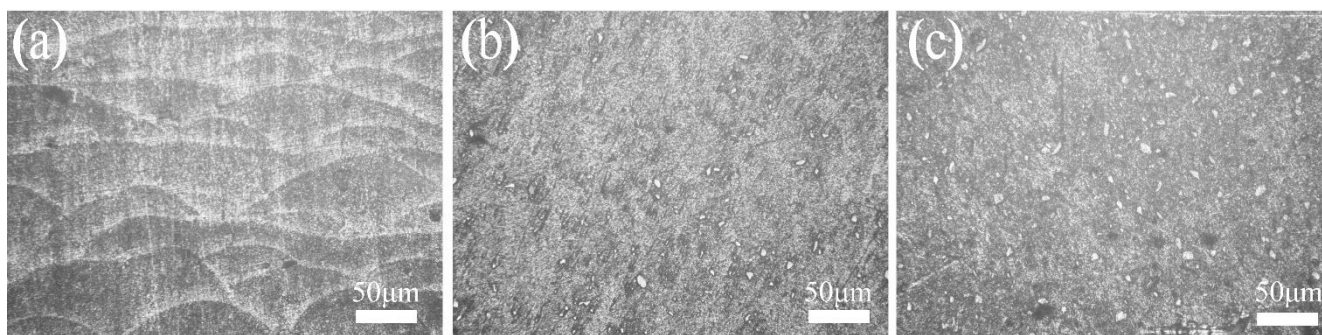


Figure 2. Metallography of aluminum matrix composites with different TiB_2 contents under 500X optical microscope (a) 0%- TiB_2 , (b) 5%- TiB_2 , (c) 15%- TiB_2

A clear molten pool outline is shown in Fig. 2 (a), white massive TiB_2 particles in Fig. 2 (b) and (c), and the outline of the molten pool begins to disappear, indicating that the molten pool increases with increasing TiB_2 content. Boundaries blur until they disappear. The reason for the disappearance of the

profile is that the addition of TiB₂ particles increases the laser absorptivity resulting in a higher processing temperature, thus making the It can be seen that the addition of TiB₂ in the Al-based composite has obvious refining effect. TiB₂ has produced an obvious effects on the microstructure refinement of Al-based materials and other alloys [12-14].

3.3 EIS of the TiB₂-AlSi10Mg composites

To further explore the effect of TiB₂ on the corrosion behavior of SLM-formed Al matrix composites, we conducted impedance tests. Fig 3 shows the Nyquist and bode plots of the 0% TiB₂ sample, the sample with 5% TiB₂ content, and the sample with 15% TiB₂ content in 3.5wt.% NaCl solution at 25 °C. The size order of the semicircle is: 0%-TiB₂/Al>15%-TiB₂/Al>5%-TiB₂/Al. In the Nyquist diagram, the semicircle represents the capacitive arc, and the larger its radius is, the better the corrosion resistance of the sample it represents [15]. It can be seen that with the addition of TiB₂, the corrosion degree of the sample increases. But the TiB₂ content continued to increase to 15% corrosion degree decreased. This law is consistent with the results obtained from the polarization curves.

From the typical EIS plot, an electrical equivalent circuit (EEC) is proposed to fit EIS results, as shown in the lower right corner of Figure 3. (This EEC is widely used in Al alloys) [16]. In this EEC, R_s stands for solution resistance, R_p stands for passive layer resistance; CPE_p stands for the constant phase element parallel to R_p , which can describe the porous nature of the material; R_{ct} stands for charge transfer resistance (corrosion pit resistance); in parallel with R_{ct} is the element CPE_{dl} , which depicts the double layer (dl) Charge transfer resistance at the sample surface. The impedance of the constant-phase element CPE is $Z_{CPE} = Y_0^{-1}(j\omega)^{-n}$, where Y_0^{-1} is the CPE constant, ω is the angular frequency (rad/s), and n is the phase angle constant and its value Between 0 (pure resistor) and 1 (pure capacitor) [17,18].

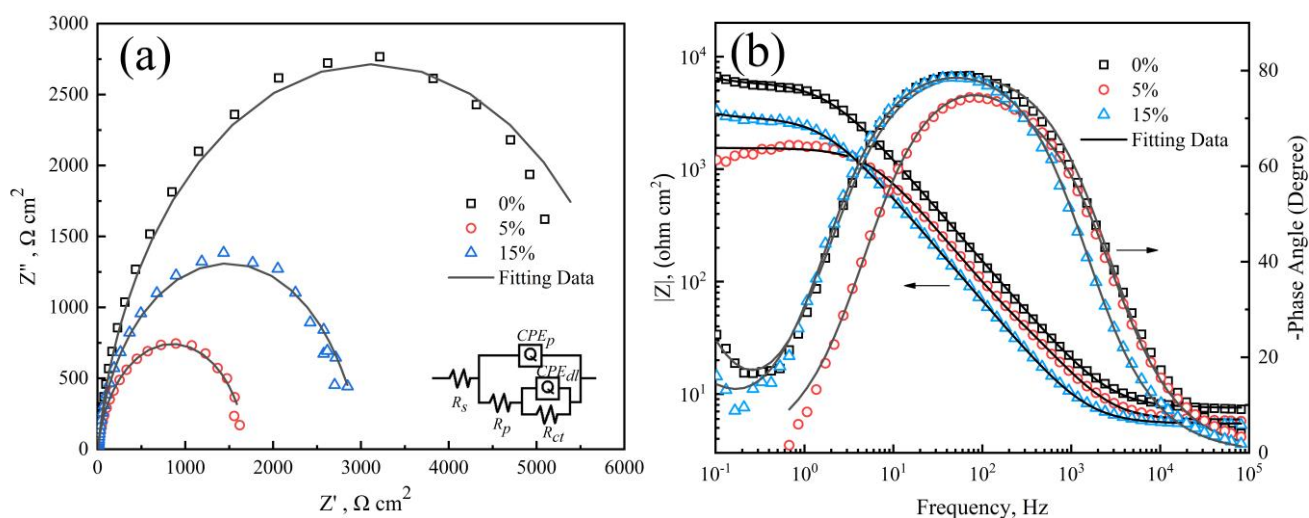


Figure 3. EIS spectra and fitting results of 0% SLM samples and 5% and 15% TiB₂ samples with frequency range from 0.01Hz to 100KHz and amplitude of 10mV (a) Nyquist plots and Electrical equivalent circuit, (b) Bode plots

Table 2. EIS fitting results were obtained using the equivalent circuit in Figure 3 (a) for all samples

Sample	R_s ($k\Omega\text{ cm}^2$)	$CPE_p \times 10^{-5}$ ($\Omega^{-1}\text{ cm}^{-2}\text{ S}^{-n}$)	n_1	R_f ($k\Omega\text{ cm}^2$)	$CPE_{dl} \times 10^{-4}$ ($\Omega^{-1}\text{ cm}^{-2}\text{ S}^{-n}$)	n_2	R_{ct} ($k\Omega\text{ cm}^2$)
Original	7.524	1.791	0.9166	6.081	6.875	1.00	21.73
5% TiB ₂	5.828	3.825	0.9189	0.1915	3.389×10^{-6}	0.951	1.488
15% TiB ₂	5.448	2.328	0.9262	2.955	2.529×10^{-3}	1.00	1.887

Table 2 shows the data obtained by fitting the EIS data through EEC. It can be found by comparing R_{ct} and R_p that the original sample without TiB₂ is $R_{ct} > R_f$, which proves that the sample mainly corrodes the surface by uniform corrosion/general corrosion; But after adding TiB₂, it was found that $R_{ct} < R_f$ of 5% and 15% samples, which indicated that the corrosion of the samples was mainly pitting [19]. The above statement can be proved in Fig. 6 SEM image. The CPE index (n) values of all samples are close to 1 indicating that the surface passivation layers of all SLMed Al-based composites exhibit pure capacitive behavior regardless of the TiB₂ content. In addition, the increase in TiB₂ content resulted in an increased in the number of weld pool boundaries which adversely affected the passivation/oxide uniformity, resulting in thinner and less uniform passivation/oxide on the specimen surface [20]. Use EIS to fit different passivation layer capacitances of the data (simple bring-in method, because the CPE obtained by fitting does not represent the actual capacitance properties of the passivation film, so we choose to simply bring in), using the relationship of plate capacitance, the passivation can be determined. The thickness of chemical film (D_{ox}):

$$D_{ox} = \frac{\varepsilon \varepsilon_0 A}{C_{eff}}$$

where ε represents the dielectric constant of the passivation layer (the dielectric constant of Al₂O₃ is generally 8.5) [21]. ε_0 represents the vacuum dielectric constant ($8.854 \times 10^{-14}\text{ F cm}^{-1}$), A represents the geometric surface area of the sample; C_{eff} represents the pure capacitance value of the passivation layer ($\mu\text{F cm}^{-2}$). In the EIS fitting data (Table 2), the order of the passivation film time constant CPE_p is: 5% > 15% > origin (simply bring in the CPE value and directly select the real capacitance value), the passivation film thickness (D_{ox}) Inversely proportional to the capacitance value (C_{eff}), the order of D_{ox} size is: 0% > 15% > 5%, which is consistent with the R_f (passivation film resistance) law.

3.4 Potentiodynamic polarization tests of the TiB₂-AlSi10Mg composites

To study the effect of adding different contents of TiB₂ to the corrosion resistance of SLM-formed aluminum matrix composites, potentiodynamic polarization tests were carried out for the three samples respectively. To ensure the accuracy and stability of the experiment, all samples were monitored for 1 h OCP in 3.5wt.% NaCl solution at 25 °C and room temperature before potentiodynamic polarization test. The anodic polarization curve (Fig.4) shows that the corrosion potential (E_{corr}) is positively shifted (corrected) in the following order: 5% sample ($E_{corr} = -0.574 \pm 0.04\text{ V}_{\text{Ag}/\text{AgCl}}$) > 15% sample ($E_{corr} = -0.591 \pm 0.05\text{ V}_{\text{Ag}/\text{AgCl}}$) > 0% sample ($E_{corr} = -0.621 \pm 0.02\text{ V}_{\text{Ag}/\text{AgCl}}$). It shows that the corrosion potential of the 5% sample is more positive, and the corrosion tendency is smaller than that of the other two samples. The small corrosion tendency of the samples containing TiB₂ is due to the increase of the reinforcement

phase, which leads to the decrease of the area fraction of the anode such as the Al matrix, and the increase of the area fraction of the cathode side, and the addition of the second phase as a fine grain makes the material in the process of processing. The size decreases, the grain boundary density increases, and the overall reactivity of the surface increases, suppressing the generation of corrosion relative to the pristine sample [19]. However, the corrosion current density (I_{corr}) increases according to the law of $0\% < 15\% < 5\%$. The Al/TiB₂ interface as the starting point of corrosion is the reason for the weakening of the corrosion resistance of Al-based composites [22]. The anodic dissolution rate increases rapidly once it occurs, and its regularity is as follows: $5\% > 15\% > 0\%$, and the regularity of a corrosion current density (I_{corr}) is consistent. TiB₂ as a large particle conductive phase as a large cathode makes the aluminum matrix easy to dissolve. Therefore, it is difficult to form a dense oxide film/passivation film after adding TiB₂ particles [23].

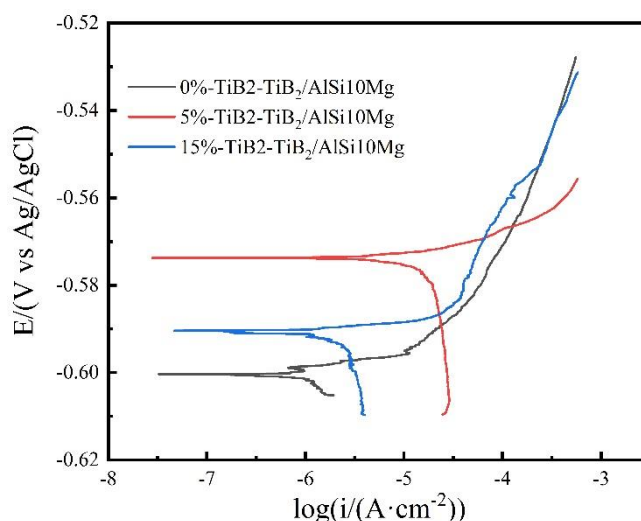


Figure 4. Polarization curves of three different TiB₂ content aluminum matrix composites prepared by SLM which scanning rate is 0.125 mV/s and the scanning range is -0.02V to 0.3V vs OCP.

Table 3. Polarization curve fitting data of three different TiB₂ content aluminum matrix composites prepared by SLM in aerated 3.5 wt.% NaCl solution.

Samples	Corrosion potential (V _{Ag/AgCl})	Corrosion current density (A/cm ²)
0%-TiB ₂ & AlSi10Mg	-0.621	1.06×10^{-6}
5%-TiB ₂ & AlSi10Mg	-0.574	2.6×10^{-5}
15%-TiB ₂ & AlSi10Mg	-0.591	1.88×10^{-6}

Figure 5 shows the SEM morphologies of the three samples after electrochemical polarization. Fig 5 (a) shows that white corrosion products are uniformly produced on the surface of the original

sample, while after adding 5% and 15% TiB_2 reinforcements, the corrosion products aggregate and increase, especially at 5%. In Fig. 5(b), it can be seen that after the polarization test of the sample added with TiB_2 , local pitting corrosion on the surface of the sample is caused, mainly around the TiB_2 reinforcement (as shown by the blue arrow), and with the increase of the pitting pit, it develops into more pitting corrosion. Severe selective corrosion [18]. After the energy spectrum test of 15% (Fig 6), it can be seen that pitting occurs around TiB_2 , especially where TiB_2 aggregates.

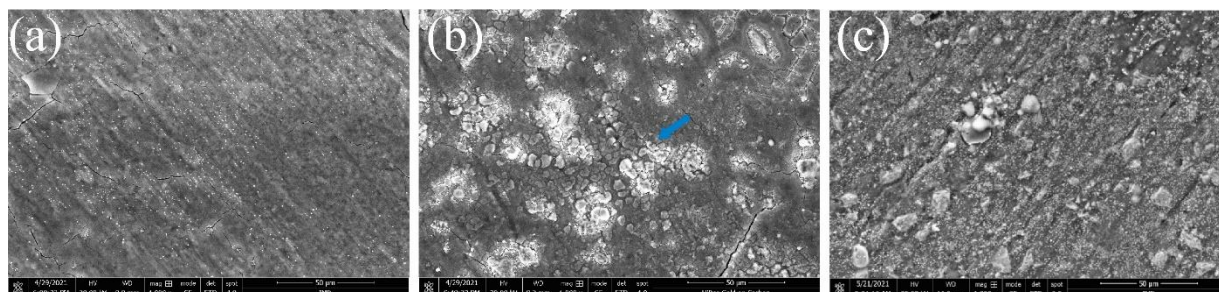


Figure 5. SEM micrographs of the sample after the polarization test: (a) 0%- $\text{TiB}_2/\text{AlSi10Mg}$, (b) 5%- $\text{TiB}_2/\text{AlSi10Mg}$, (c) 15%- $\text{TiB}_2/\text{AlSi10Mg}$

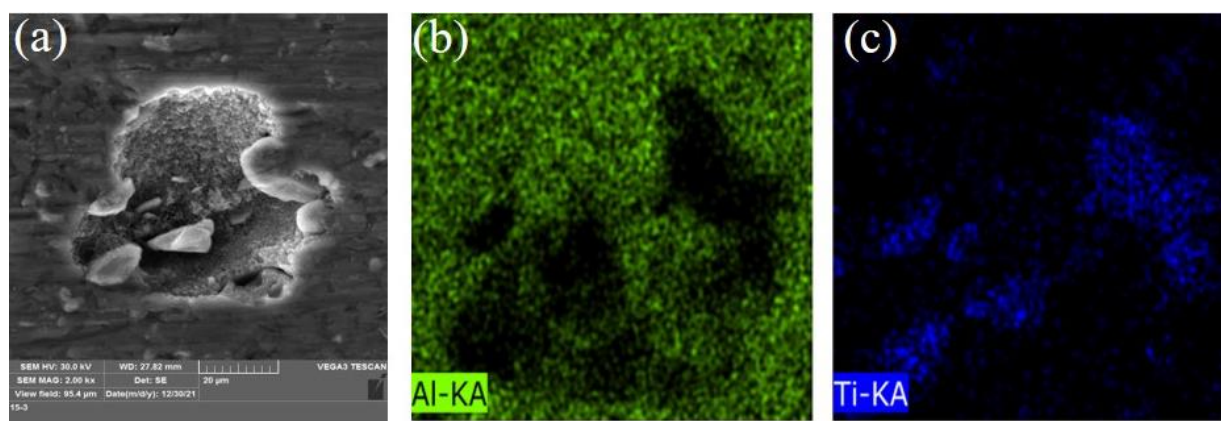


Figure 6. Energy dispersive spectroscopy mapping of 15% sample after the polarization test: (a) Electron image, (b) Al, (c) Ti

4. CONCLUSION

In this paper, AlSi10Mg composites manufactured by selective laser melting (SLM) technology are taken as the research object, and the effect of TiB_2 contents on the corrosion behavior of Al-based materials is explored. The main experimental conclusions are obtained:

- (1) From the metallographic images, it can be known that the sample presents an obvious molten pool profile before adding TiB_2 , but after adding TiB_2 , the molten pool profile disappears and TiB_2 is evenly distributed in the matrix in the form of small particles. The SEM images show that the original sample without TiB_2 is in uniform corrosion state after corrosion test. The sample added 5 % / 15 %

showed pitting. The energy spectrum shows that pitting mainly occurs around TiB₂.

- (2) The EIS results show that the original aluminum matrix composite presents a larger arc-tolerant radius, showing better corrosion resistance than the other two samples with TiB₂. At the same time, the impedance fitting data and the passivation layer thickness formula can prove that the passivation layer thickness sequence is 0 % > 15 % > 5 %.
- (3) The corrosion potential sequence of the sample is 0 % < 15 % < 5 %. The polarization curve shows that the corrosion potential of the sample moves forward after adding TiB₂. The addition of TiB₂ effectively improves the overall stability of the sample surface and reduces the corrosion tendency of the sample. From the corrosion current density of 0 % (1.06×10^{-6}) < 15 % (1.88×10^{-6}) < 5 % (2.6×10^{-5}), adding TiB₂ in the sample can increase the corrosion current density of the sample, and the pitting corrosion becomes serious. Considering that adding 15 % TiB₂ to improve other mechanical properties of the material can effectively enhance the corrosion resistance of the sample, and has similar pitting resistance to the base metal.

ACKNOWLEDGMENT

This work was supported by Liaoning Province Department of Education Research Funding Project(NO. LJKZ0385) and Scientific Research Funds Project of Liaoning Education Department of China (No. L2019049).

References

1. L. Thijs, K. Kempen, J. P. Kruth, and J. Van Humbeeck, *Acta Mater.*, 61 (2013) 1809.
2. D. Buchbinder, H. Schleifenbaum, S. Heidrich, W. Meiners and J. Bültmann, *Physics Procedia*, 12 (2011) 271.
3. D. Gu, *Laser Additive Manufacturing of High-Performance Materials*, Springer Berlin Heidelberg, (2015).
4. K. N. Amato, S. M. Gaytan, L. E. Murr, E. Martinez, P. W. Shindo, J. Hernandez, S. Collins and F. Medina, *Acta Mater.*, 60 (2012) 2229.
5. S. Z. Uddin, L. E. Murr, C. A. Terrazas, P. Morton, D. A. Roberson, and R. B. Wicker, *Addit. Manuf.*, 22 (2018) 405.
6. K. G. Prashanth, S. Scudino, and J. Eckert, *Acta Mater.*, 126 (2017) 25.
7. Z. Zhao, P. Bai, W. Du, B. Liu, and Z. Guo, *Carbon*, 170 (2020).
8. Z. Liu, T. Zhu, Y. Jia, D. Song, N. Zhou and K. Zheng, *Mater. Res. Express*, 8 (2021) 046506.
9. H. Rao, S. Giet, K. Yang, X. Wu, Davies, and Chris H. J, *Mater. Des.*, (2016).
10. M. Rafieezad, M. Mohammadi, A. Gerlich, and A. Nasiri, *Corros. Sci.*, 178 (2021) 109073.
11. X. Xie, B. Hosni, C. Chen, H. Wu, and H. Liao, *Surf. Coat. Technol.*, 404 (2020).
12. McCartney, D. G, *Metallurgical Reviews*, 34 (1989) 247.
13. B. S. Murty, S. A. Kori, and M. Chakraborty, *Metallurgical Reviews*, 47 (2002) 3.
14. Z. Fan, Y. Wang, Y. Zhang, T. Qin, and X.R. Zhou, G.E, *Acta Mater.*, 84 (2015) 292.
15. ME Orazem, and B Tribollet, *Electrochemical Impedance Spectroscopy*, New Jersey, (2008) 383.
16. X. Xie, B. Hosni, C. Chen, H. Wu, and H. Liao, *Surf. Coat. Technol.*, 404 (2020).
17. R. Arrabal, B. Mingo, A. Pardo, M. Mohedano, E. Matykina, and I. Rodriguez, *Corros. Sci.*, 73 (2013) 342.
18. P. Fathi, M. Rafieezad, X. Duan, M. Mohammadi, and AM Nasiri, *Corros. Sci.*, 157 (2019) 126.

19. M. Rafieezad, M. Mohammadi, A. Gerlich, and A. Nasiri, *Corros. Sci.*, 178 (2021) 109073.
20. RI Revilla, Y. Rojas, and ID Graeve, *J. Electrochem. Soc.*, 166 (2019) 530.
21. AG Rao, VA Katkar, G Gunasekaran, VP Deshmukh, N Prabhu, and BP Kashyap, *Corros. Sci.*, 83 (2014) 198.
22. C. Vargel, M. Jacques and M. P. Schmidt, *Corrosion of aluminum*, Elsevier Science, (2004).
23. N. Dai, J. Zhang, Y. Chen, and L. C. Zhang, *J. Electrochem. Soc.*, 164 (2017) 428.

© 2022 The Authors. Published by ESG (www.electrochemsci.org). This article is an open access article distributed under the terms and conditions of the Creative Commons Attribution license (<http://creativecommons.org/licenses/by/4.0/>).